Mathematical Development of Duty Cycles Computing to Four Switches 2ϕ-Inverter Advanced SVM for TPIM Drive

Intissar Moussa*‡, Adel Khedher*

* Université de Sousse, Ecole Nationale d'Ingénieurs de Sousse, LATIS-Laboratory of Advanced Technology and Intelligent Systems, 4023, Sousse, Tunisia;

(intissar.moussa.essoussi@gmail.com, adel_kheder@yahoo.fr)

‡ Corresponding Author; Intissar Moussa, BP 264 Sousse Erriadh, Tel: +216 369 500, Fax: +216 73 369 506, intissar.moussa.essoussi@gmail.com

Received: 14.04.2022 Accepted: 30.05.2022

Abstract- This paper deals with a mathematical development of four-switch inverter duty cycles computing for two-phase induction motors drive. The proposed proof serves to explain the steps to be followed from the reference voltage graphical representation to the switching sequence determination. Two structures of 2ϕ-inverter two-phase induction motor (TPIM) associations such as two-leg four switches and two-leg six switches are briefly presented. Hence, the difference between the space vector modulation control strategies of these alternative current motor drives is analyzed. The considered 2ϕ-inverter topology is carefully detailed to facilitate the computing method comprehension for TPIM speed control in order to perform their switching sequences generation and therefore the hardware implementation complexity through numerical boards. By this structure, wind energy emulation, electric traction and photovoltaic pumping fields can be targeted.

Keywords Four switch 2ϕ-Inverter, Two-Phase Induction Motor, Advanced SVM technique, Mathematical proof, Hardware implementation.

1. Introduction

Induction machines are almost used in several applications namely electricity production process, electrical traction, PV pumping and wind energy emulation [1,2]. These electrical machines operating principle is based on the interaction between the magnetic fields and the currents flowing in the machine windings. The winding constructions and connections together with the currents and voltages injected into them determine the operating modes and the electrical machine type. Many schemes for vector-controlled induction motor (IM) drives have been suggested for nearly a decade [3].

Within an inverter, the switches switching ensure the energy transfer between a DC power source and AC load. They define the relation between closing and opening intervals of each switch. As far as alternative waveforms are concerned, sinusoidal quantities, remain the most difficult to reach since they are the most desired. Therefore, pulse width modulation (PWM) control techniques are strongly used. Numerical PWM technology is constantly optimizing and renovating, which passed from the Sine Pulse Width Modulation (SPWM) to the widely used Space Vector Pulse Width Modulation (SVPWM) at present, with the modern power electronic technology development [4]. The SVPWM is a special switch trigger order and pulse width combination of voltage source inverter power device, which its performance in terms of advanced and accurate PWM computation has been proven theoretically and practically. This technique was known by its output voltage low-order harmonic component, DC power high utilization, low switch loss and simple algorithm that can be easily implemented in a digital device. Owing to the superior performance, the SVPWM, known as SVM, has been widely used in all kinds of inverter circuits [5]. Different inverter-IM association topologies have been studied and developed such as four switch inverter-three-phase induction motor, four switch inverter-two-phase induction motor, six switch inverter-

three-phase induction motor and six switch inverter-two-phase induction motor [6]. Especially, where a 3ϕ supply is not available and in low/middle power level fields, the two-phase induction motors have been employed which needs an auxiliary winding use for adjustable speed control application. Hence, operation over a wide speed range with variable frequency drives is required. In this paper, an advanced SVM technique for two-phase induction motor is considered to minimize the output current ripple and torque oscillation. In order to better assimilate the switch states and facilitate the hardware implementation task, a time durations computing detailed mathematical proof is presented. This demonstration can be followed, as an approach, to elaborate several 2ϕ-inverter-IM association topologies switching periods.

The paper starts with two structure of 2ϕ-inverter TPIM association topologies. After that the graphical representation and the advanced SVM demonstration are detailed for 2ϕ-inverter-TPIM association to determine the times durations and hence the duty cycles for switching sequence generating. Software and hardware simulation result have been carried out to validate the proposed control technique for wind turbine emulation.

2. Two-Phase Inverter-TPIM Association Topologies

For TPIM, there are two drive types of 2ϕ-inverters namely two-leg four switches and two-leg six switches. A two-leg inverter consists of a center-tapped dc link supplied by diode rectifier and four switches as illustrated by Fig.1a or two switches and two diodes used for a boost rectifier while the rest of switches and diodes form the two-leg inverter as shown in Fig.1b.

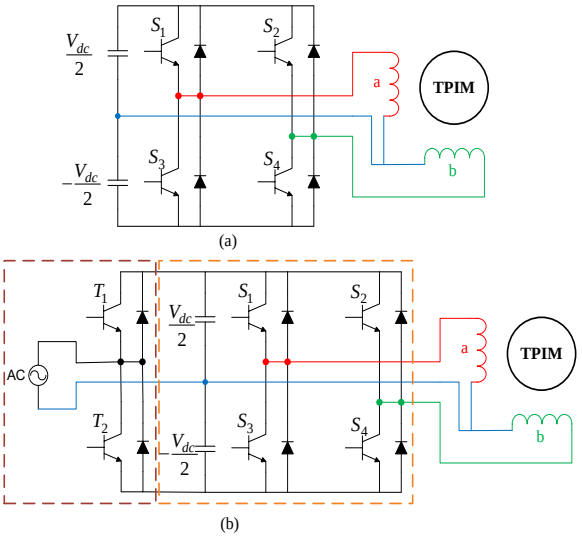

Fig. 1. Two-leg TPIM drives structures: (a) Four switches inverter, (b) six switches inverter.

Known as six switch 2ϕ-inverter, this structure is strongly recommended for power factor correction. Hence, as illustrated by Fig.2, an exact square is formed by four space vector that are evenly distributed at 90° intervals with a length of $\frac{V_{dc}}{\sqrt{2}}$. This method requires a consolidate representation to ensure the advanced carrier-based SVM implementation since it is devoid of zero vectors in the complex plane.

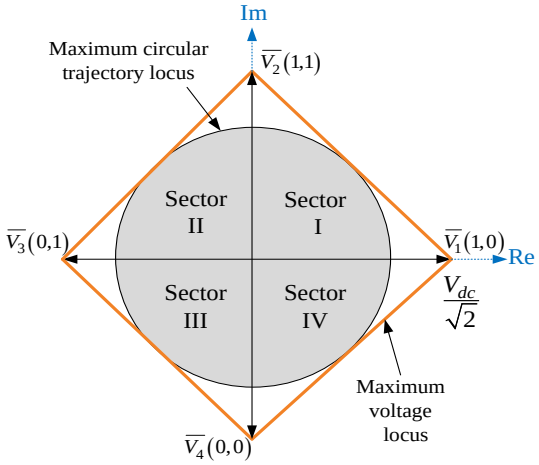

Fig. 2. Four space vectors distribution of two-leg inverter.

The switching states are given in the two-log inverter when the four switches are adjusted, as depicted by Fig.3. Hence, the space vectors are generated, based on the four possible combination.

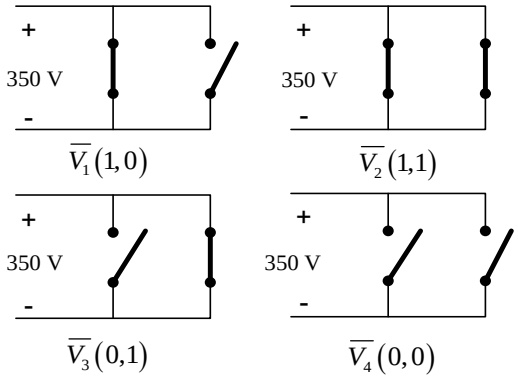

Fig. 3. Two-leg inverter switching states.

3. Mathematical Proof of the Advanced SVM Technique

The SVM technique is difficult to realize for the two-leg inverter because it doesn't have zero space vectors as the three/four-leg inverter have. Hence, an appropriate space vectors adjustment is required to establish the switching signals in order to ensure the TPIM speed drive. In this section, based on the space vectors graphical distribution in the complex plane, a mathematical proof has been proposed to carry out the 2ϕ-inverter advanced SVM without zero vectors. Figure 4 presents the location of the reference vector, V^*, in Sector I, which its module corresponds to AC,

taking into account the model sectors and the corresponding time durations.

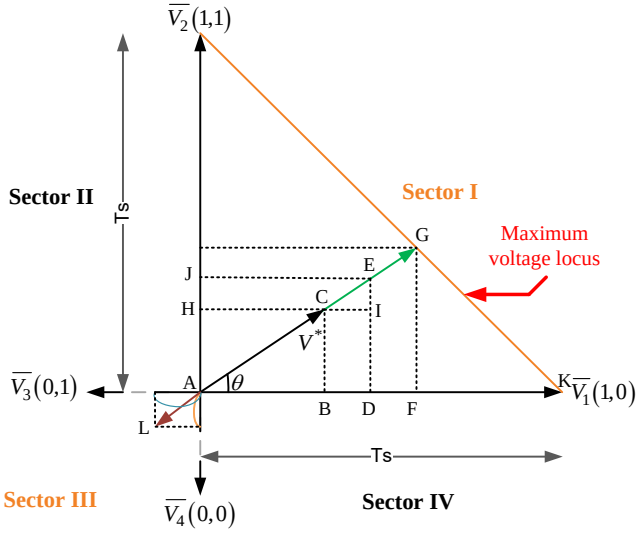

Fig. 4. Graphic representation for the 2ϕ-inverter advanced SVM switching times determining.

The control voltage vector spatial logic distribution over two switch sampling period is given by Fig.5. Indeed, the reference vector is divided into four voltage space vectors which V_1, V_2 are adjacent to V^* in the main sector (sector I) and V_3, V_4 are the restraint reference vectors in the diagonal sector (sector III). The sampling interval T_s is spent in the main and diagonal sector during times that matches AK distance in order to allow the reference vector arrives at the maximum voltage locus and since there is no zero vector. A new reference vector is formed by adding AC to CE distances.

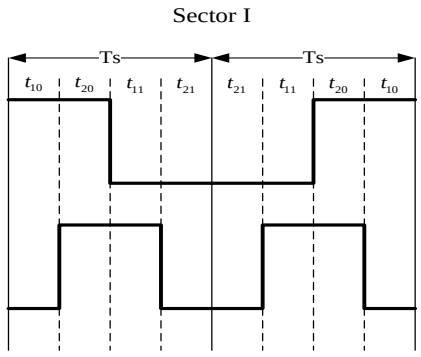

Fig. 5. Spatial logic distribution of the advanced SVM over two switch sampling period.

CG represents the difference between the reference vector module AC and the maximum voltage locus AG. Let AE denotes "the modified reference vector module". In this case, the vector module (EC) so called "the restraint vector module" should be added in the diagonal sector in opposite direction to AC, in order to restraint it to the modified reference vector module.

The sampling times relevant distance for the new reference vector in sector I, whereas AD=AB+BD and AJ=AH+HJ, is expressed as:

$$AK=AD+AJ+BD+HJ \tag{1}$$

Where,
AD and AJ, that are respectively the time durations spent on V_1, V_2 for the modified reference vector module, are distances equivalent respectively to t_{10} and t_{20}. The four time durations are solved by the following detailed process. As illustrated by Fig. 4, three triangles such as ADE, AFG and CIE have been chosen to perform the proof. At first, in order to determine the maximum space vector module to the square locus, the AFG triangle is considered. By using the trigonometric functions definition, sine and cosine are expressed as:

$$\begin{cases} \cos\theta = \dfrac{AD+FD}{\left|\overrightarrow{AC}+\overrightarrow{CG}\right|} \\ \sin\theta = \dfrac{AJ+HJ}{\left|\overrightarrow{AC}+\overrightarrow{CG}\right|} \end{cases} \tag{2}$$

As well:

$$\begin{cases} \left|\overrightarrow{AC}+\overrightarrow{CG}\right| = \dfrac{AD+FD}{\cos\theta} \\ \left|\overrightarrow{AC}+\overrightarrow{CG}\right| = \dfrac{AJ+HJ}{\sin\theta} \end{cases} \tag{3}$$

The Eq. (3) can be rewritten as follows:

$$\begin{cases} \dfrac{1}{\cos\theta}\left|\overrightarrow{AC}+\overrightarrow{CG}\right| = \dfrac{AJ+HJ}{\sin\theta\times\cos\theta} \\ \dfrac{1}{\sin\theta}\left|\overrightarrow{AC}+\overrightarrow{CG}\right| = \dfrac{AD+FD}{\sin\theta\times\cos\theta} \end{cases} \tag{4}$$

By adding the two system equations, the following equation is obtained:

$$\left|\overrightarrow{AC}+\overrightarrow{CG}\right|\left(\frac{1}{\sin\theta}+\frac{1}{\cos\theta}\right) = \frac{1}{\cos\theta\cdot\sin\theta}\left(AD+FD+AJ+HJ\right) \tag{5}$$

Hence, the maximum space vector is given by:

$$\left|\overrightarrow{AC}+\overrightarrow{CG}\right| = \frac{AK}{\cos\theta+\sin\theta} \tag{6}$$

Thus:

$$\left|\overrightarrow{AC}+\overrightarrow{CG}\right|=\frac{V_{dc}}{\sqrt{2}}\frac{1}{\cos\theta+\sin\theta} \quad (7)$$

Since $\overrightarrow{AC}$ and $\overrightarrow{CG}$ are two collinear vectors in the same direction, the following expression is written as:

$$\left|\overrightarrow{AC}+\overrightarrow{CG}\right|=\left|\overrightarrow{AC}\right|+\left|\overrightarrow{CG}\right| \quad (8)$$

Thus, by substituting Eq. (7) into Eq. (8), the module of the difference vector, $\left|\overrightarrow{CG}\right|$, is given by:

$$\left|\overrightarrow{CG}\right|=\frac{V_{dc}}{\sqrt{2}}\frac{1}{\left(\cos\theta+\sin\theta\right)}-\left|\overrightarrow{AC}\right| \quad (9)$$

By dividing Eq. (7) by 2, the result is obtained as:

$$\left|\frac{\overrightarrow{AC}}{2}+\frac{\overrightarrow{CG}}{2}\right|=\frac{V_{dc}}{2\sqrt{2}}\frac{1}{\cos\theta+\sin\theta} \quad (10)$$

Since, $\left|\frac{\overrightarrow{AC}}{2}\right|=\left|\overrightarrow{AC}-\frac{\overrightarrow{AC}}{2}\right|$, the modified reference vector module in the main sector is expressed as:

$$\left|\overrightarrow{AC}-\frac{\overrightarrow{AC}}{2}+\frac{\overrightarrow{CG}}{2}\right|=\left|\overrightarrow{AC}+\overrightarrow{CE}\right|-\left|\frac{\overrightarrow{AC}}{2}\right| \quad (11)$$

Based on Eq. (10) and Eq. (11), it is deduced:

$$\left|\overrightarrow{AC}+\overrightarrow{CE}\right|-\left|\frac{\overrightarrow{AC}}{2}\right|=\frac{V_{dc}}{2\sqrt{2}}\frac{1}{\cos\theta+\sin\theta} \quad (12)$$

Where, $\left|\frac{\overrightarrow{CG}}{2}\right|=\left|\overrightarrow{CE}\right|$

From Eq.(10), the following expression is given as :

$$\left|\overrightarrow{CE}\right|=\frac{V_{dc}}{2\sqrt{2}}\frac{1}{\cos\theta+\sin\theta}-\left|\frac{\overrightarrow{AC}}{2}\right| \quad (13)$$

By applying the collinearity theorem between two vectors of opposite direction, $\overrightarrow{CE}$ and $\overrightarrow{AL}$ have the same module and consequently, the restraint vector absolute value in the diagonal sector is:

$$\left|\overrightarrow{AL}\right|=\frac{V_{dc}}{2\sqrt{2}}\frac{1}{\cos\theta+\sin\theta}-\left|\frac{\overrightarrow{AC}}{2}\right| \quad (14)$$

Now, moving to the ADE triangle, cosine and sine functions are defined as:

$$\begin{cases}\cos\theta=\dfrac{AD}{\left|\overrightarrow{AC}+\overrightarrow{CE}\right|}\\ \sin\theta=\dfrac{AJ}{\left|\overrightarrow{AC}+\overrightarrow{CE}\right|}\end{cases} \quad (15)$$

Hence,

$$\begin{cases}AD=\left|\overrightarrow{AC}+\overrightarrow{CE}\right|\cos\theta\\ AJ=\left|\overrightarrow{AC}+\overrightarrow{CE}\right|\sin\theta\end{cases} \quad (16)$$

According to the relation between the time durations equivalent distance and the modified reference vector module in the main sector, $\frac{AK}{AD}$ and $\frac{AK}{AJ}$ are written, and the following equations are obtained as:

$$\begin{cases}\dfrac{AK}{AD}=\dfrac{\frac{V_{dc}}{\sqrt{2}}}{\left|\overrightarrow{AC}+\overrightarrow{CE}\right|\cos\theta}\\ \dfrac{AK}{AJ}=\dfrac{\frac{V_{dc}}{\sqrt{2}}}{\left|\overrightarrow{AC}+\overrightarrow{CE}\right|\sin\theta}\end{cases} \quad (17)$$

The time durations equivalent distances AB and AJ respectively can be solved by substituting Eq. (11) into Eq. (17) as follows:

$$AD=\frac{AK\left|\overrightarrow{AC}+\overrightarrow{CE}\right|\cos\theta}{\frac{V_{dc}}{\sqrt{2}}} \quad (18)$$

Also:

$$AD=\frac{\sqrt{2}AK}{V_{dc}}\left|\overrightarrow{AC}+\overrightarrow{CE}\right|\cos\theta \quad (19)$$

After developing,

$$AD=\frac{\sqrt{2}AK}{V_{dc}}\left[\frac{V_{dc}}{2\sqrt{2}}\frac{1}{\cos\theta+\sin\theta}+\left|\frac{\overrightarrow{AC}}{2}\right|\right]\cos\theta \quad (20)$$

Otherwise,

$$AJ = \frac{AK\left|\overrightarrow{AC}+\overrightarrow{CE}\right|\sin\theta}{\frac{V_{dc}}{\sqrt{2}}} \quad (21)$$

Thus,

$$AJ = \frac{\sqrt{2}AK}{V_{dc}}\left|\overrightarrow{AC}+\overrightarrow{CE}\right|\sin\theta \quad (22)$$

Finally Eq. (22) is rewritten as:

$$AJ = \frac{\sqrt{2}AK}{V_{dc}}\left[\frac{V_{dc}}{2\sqrt{2}}\frac{1}{\cos\theta+\sin\theta}+\left|\frac{\overrightarrow{AC}}{2}\right|\right]\sin\theta \quad (23)$$

In order to determine the time durations equivalent distances in the diagonal sector, cosine and sine functions are solved based on the CIE triangle as:

$$\begin{cases}\cos\theta = \dfrac{BD}{\left|\overrightarrow{CE}\right|}\\ \sin\theta = \dfrac{HJ}{\left|\overrightarrow{CE}\right|}\end{cases} \quad (24)$$

Therefore, Eq. (24) gives:

$$\begin{cases}BD = \overrightarrow{CE}\cos\theta = \left|\overrightarrow{AL}\right|\cos\theta\\ HJ = \left|\overrightarrow{AL}\right|\sin\theta\end{cases} \quad (25)$$

According to the relation between the time durations equivalent distance and the restraint reference vector module in the diagonal sector, $\frac{AK}{BD}$ and $\frac{AK}{HJ}$ are written, therefore the equation is given as follows:

$$\begin{cases}\dfrac{AK}{BD} = \dfrac{\frac{V_{dc}}{\sqrt{2}}}{\left|\overrightarrow{AL}\right|\cos\theta}\\ \dfrac{AK}{AJ} = \dfrac{\frac{V_{dc}}{\sqrt{2}}}{\overrightarrow{AL}\sin\theta}\end{cases} \quad (26)$$

The time durations t_{11} and t_{21} match distances BD and HJ respectively can be solved, by substituting Eq. (11) into Eq. (26) as follows:

$$BD = \frac{AK\left|\overrightarrow{AL}\right|\cos\theta}{\frac{V_{dc}}{\sqrt{2}}} \quad (27)$$

Which leads to:

$$BD = \frac{\sqrt{2}AK}{V_{dc}}\left[\frac{V_{dc}}{2\sqrt{2}}\frac{1}{\cos\theta+\sin\theta}-\left|\frac{\overrightarrow{AC}}{2}\right|\right]\cos\theta \quad (28)$$

Otherwise,

$$HJ = \frac{AK\left|\overrightarrow{AL}\right|\sin\theta}{\frac{V_{dc}}{\sqrt{2}}} \quad (29)$$

Which yields to:

$$HJ = \frac{\sqrt{2}AK}{V_{dc}}\left[\frac{V_{dc}}{2\sqrt{2}}\frac{1}{\cos\theta+\sin\theta}-\left|\frac{\overrightarrow{AC}}{2}\right|\right]\sin\theta \quad (30)$$

The four time durations and the four space vectors should be adjusted by four switches during T_s to generate the appropriate switching sequence in the 2ϕ-inverter advanced SVM for TPIM drive as:

$$T_s\overline{V}^{*} = t_{10}\overline{V}_1 + t_{20}\overline{V}_2 + t_{11}\overline{V}_3 + t_{21}\overline{V}_4 \quad (31)$$

The duty cycles d_1, d_2, d_3 and d_4 are computed by dividing the time durations by T_s as follows:

$$\begin{cases}d_1 = \dfrac{AD}{AK} = \dfrac{\sqrt{2}}{V_{dc}}\left[\dfrac{V_{dc}}{2\sqrt{2}\left(\cos\theta+\sin\theta\right)}+\left|\dfrac{\overrightarrow{AC}}{2}\right|\right]\cos\theta\\ d_2 = \dfrac{AJ}{AK} = \dfrac{\sqrt{2}}{V_{dc}}\left[\dfrac{V_{dc}}{2\sqrt{2}\left(\cos\theta+\sin\theta\right)}+\left|\dfrac{\overrightarrow{AC}}{2}\right|\right]\sin\theta\\ d_3 = \dfrac{BD}{AK} = \dfrac{\sqrt{2}}{V_{dc}}\left[\dfrac{V_{dc}}{2\sqrt{2}\left(\cos\theta+\sin\theta\right)}-\left|\dfrac{\overrightarrow{AC}}{2}\right|\right]\cos\theta\\ d_4 = \dfrac{HJ}{AK} = \dfrac{\sqrt{2}}{V_{dc}}\left[\dfrac{V_{dc}}{2\sqrt{2}\left(\cos\theta+\sin\theta\right)}-\left|\dfrac{\overrightarrow{AC}}{2}\right|\right]\sin\theta\end{cases} \quad (32)$$

4. Hardware Implementation and Results

In order to verify this control strategy reliability and performance, the two-leg 2ϕ-inverter structure for TPIM drive is considered to emulate a wind turbine static and dynamic characteristics for research laboratory purpose. Hence, the advanced SVM technique, the TPIM vector control and the turbine mathematical model, which gives the reference speed for the system, have been embedded for system digital control as depicted in Fig.6.

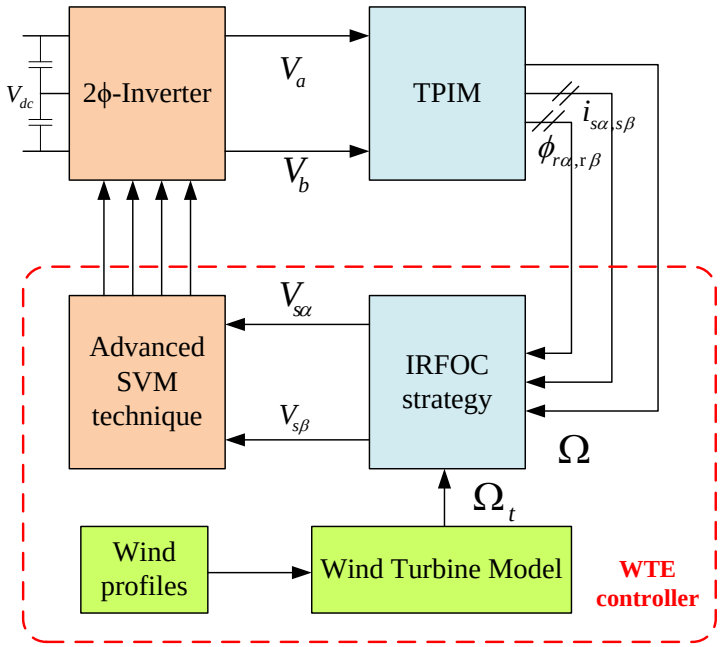

Fig. 6. WTE block diagram based on 2ϕ-inverter advanced SVM for TPIM drive.

In order to validate the proposed wind turbine emulator (WTE) closed-loop control response under dynamic conditions, software and hardware computer models have been designed. The control scheme, allowing the WTE to react as a real turbine, has the role to generate two-phase voltages balance for the TPIM drive based on the advanced SVM and the indirect rotor field-oriented control (IRFOC) methods. The Xilinx high-level XSG tools is used to prototype rapidly the control architecture VHDL programming to be implemented on FPGA. An intellectual property (IP) module, which consists of many functional blocks such us look-up table, CORDIC and counter, has been carefully configured to produce the corresponding output signals with respect to the timing, modularity, algorithm and FPGA implementation constraints to match better control algorithm for the power circuit stage. Results are shown in Fig.7. It shows that mechanic, electromagnetic and electric quantities are well obtained. The turbine reference speed changes according to the wind speed and after 0.2 s the system steady-state is established despite the wind fluctuations. The TPIM speed is accelerated smoothly to follow its reference value with nearly zero steady state and transient errors. The stator currents keep a sinusoidal shapes and vary according the speed and load torque. The rotor fluxes oscillate around their reference value equal to 0.7 Wb and keep a quadrature sinusoidal form in αβ frame. Therefore, the FPGA-based digital control robustness of the proposed WTE design based on 2ϕ-inverter advanced SVM for TPIM drive was confirmed by these obtained waveforms.

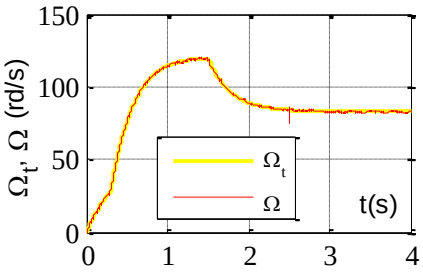

(a)

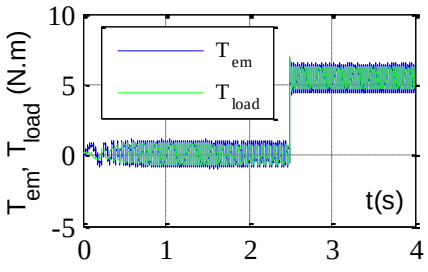

(b)

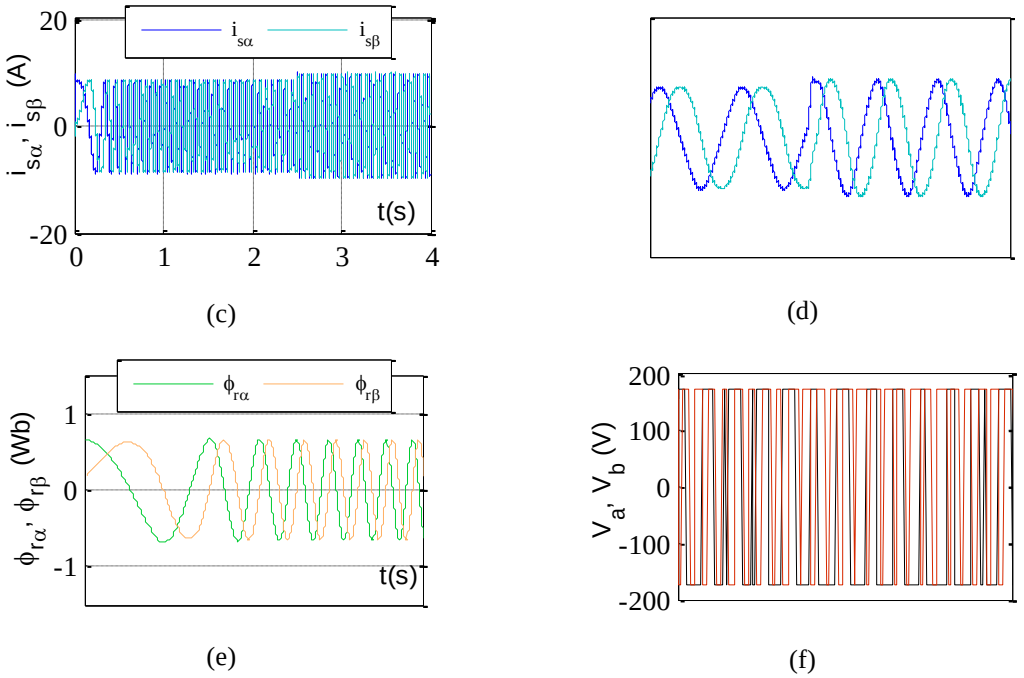

Fig. 7. Hardware implementation results of the proposed WTE structure: (a) Turbine and TPIM speeds, (b) TPIM electromagnetic and load torques, (c) TPIM stator currents, (d) Zoom of the TPIM stator currents, (e) TPIM rotor fluxes (f) Generated output voltages.

5. Conclusion

In this paper, a mathematical proof of 2ϕ-inverter advanced SVM technique for TPIM drive is investigated. Two-leg 2ϕ-inverter TPIM association types are presented which include the four switches and the six switches topologies. The two-leg one is adopted to be detailed as it is more complex in terms of control signals hardware implementation. Since there are no zero space vectors, a reference voltage vector change is realized by adjusting four space vectors in the main and diagonal corresponding sectors. Trigonometric function definitions and collinearity theorem have been used for the time durations and therefore duty cycles demonstration. This study clarifies the computational steps for an SVM control technique and can be considered in different fields such as electrical traction, PV pumping and wind energy emulation based on TPIM. To validate this control method effectiveness, both software and hardware results have been carried out for wind profile emulation in research laboratory.

Acknowledgements

This research received no external funding and the authors declare no conflict of interest.

References

[1] Jr, C.R. Schmidlin, F.K. de Araújo Lima, F.G. Nogueira, C.G.C. Branco, and F.L. Tofoli, "Reduced-order modeling approach for wind energy conversion systems based on the doubly-fed induction generator", Electric Power Systems Research, vol. 192, p. 106963, 2021. (Article)

[2] H.M. Kojabadi, L. Chang and T. Boutot, "Development of a novel wind turbine simulator for wind energy conversion systems using an inverter-controlled induction motor", IEEE Trans. Energy Conv., vol. 19, pp. 547-552, 2004. (Article)

[3] D.H. Jang, "Problems incurred in a vector-controlled single-phase induction motor, and a proposal for a vector-controlled two-phase induction motor as a replacement", IEEE Trans. Power Electronics, vol. 28, pp. 526-536, 2012. (Article)

[4] J. Yu, R. Yu, H. Wen, X. Lin, and K. Hu, "Simplified SVPWM-based SoC balancing strategy for three-phase cascaded H-bridge multilevel converter in off-grid energy storage systems", Inter. J. Electrical Power & Energy Systems, vol. 137, p. 107474, 2022. (Article)

[5] A.G.M.A. Aziz, H. Rez, and A.A.Z. Diab, "Robust Sensorless Model-Predictive Torque Flux Control for High-Performance Induction Motor Drives", Mathematics, vol. 9, p. 403, 2021. (Article)

[6] D.H. Jang, "PWM methods for two-phase inverters", IEEE Indus. Applications magazine, vol. 13, pp. 50-61, 2007. (Article)